Chapter 1

Introduction

The typical time for chemical bond cleavage and reformation is situated in the range of a few femtoseconds to some picoseconds, dictated by the motion of molecular fragments on their potential energy surfaces. Besides analysis of chemical reactions using ultrashort laser pulse spectroscopy [1–3], the possibility to control the reaction arose [4]. In most of these schemes, a *coherence* in the reacting system is a precondition in achieving the goal, and therefore the term "coherent control" has been applied.

By *coherence*, a well defined phase relation among quantum mechanical wave functions is meant. For molecular systems, the wave functions are divided into electronic, vibrational and rotational parts. The coherent superposition of corresponding eigenstates is called an electronic, vibrational or rotational *wave packet* [5].

Coherently coupled eigenstates can show interference patterns. In the optical double slit experiment, the interference pattern can only be observed if the relative phase of the field emerging from the two slits is stable. In an analogous way, one can construct an interference pattern of two quantum states with fixed relative phases. The optical analogy for the interference of more than two eigenstates is a multiple slit or grating experiment. Due to these formal similarities, the field of coherent quantum phenomena is often called "quantum optics" [6]. Coherent control schemes exploit the interference patterns of wave functions to control the output of a reaction. For example, the "Tannor-Rice" method [7,8] uses the interference of intramolecular vibrational wave functions to achieve a control goal.

The decay of coherence is called *decoherence* or *dephasing*.[1] It is induced by the coupling of the coherent system to an environment which provides statistical fluctuations on the phases of eigenstates. This leads to attenuated interferences among the eigenstates.

Dephasing, used here synonymously with decoherence, destroys the premise of coherent control. For an application, the dephasing times of the molecule involved have to be taken into account. In case of free molecules in the vacuum, the electronic, vibrational, and rotational dephasing times are much longer than the timescales of chemical reactions. Molecules solvated in a liquid or solid environment show considerably shorter dephasing times in the range of femto- to picoseconds. The trend in coherent control of chemical reactions moves in the direction of multidimensional systems in solution, often with biological relevance. Besides dephasing and dissipation of energy, the *dispersion* of wave packets is a crucial process. Wave packets on *anharmonic* potentials (which all relevant molecular potentials are) undergo a broadening, however without a loss of phase memory.

This study aims at establishing a basic model for multidimensional systems like organic dyes or biomolecules in solution, and to isolate dissipation, dephasing and dispersion processes. The insight gained in the model can clarify the preconditions for the observation of coherences in complex systems.

[1] The terminology will be specified in section 2.2.4.

Rare Gas Solids (RGS) present conceptually simple hosts. They have a large ionization energy which allows for using high intensity laser pulses. The rare gas atoms are spherical because of their closed electronic shells and they form face centered cubic (fcc) crystals at low temperature [9]. The phonon dispersion relations and optical properties of the crystals are well studied [10–12]. The rare gas atoms are chemically inert, thus one can use adapted gas phase potentials for the molecular dopants.

The molecule in RGS system, studied in this thesis, is chosen under the constraint of an ultrafast dissipation and dephasing, since this is generally the case for large molecules in solutions. In RGS, excited electronic states of halogens undergo such fast processes because their vibrational level spacing is close to the Debye frequency. A variety of halogens has been studied before in RGS.

The molecule can be described as a one dimensional vibronic quantum system, if its rotation is blocked in the RGS. The ClF molecule is sitting on a single-substitutional site in RGS [13–19] and undergoes ultrafast angular randomization after excitation [20] and is therefore not appropriate. First experiments on Cl_2, sitting on a double-substitutional site in RGS, indicate it to be a suitable system under the above mentioned constraints. However, the anharmonicity and resulting dispersion on the electronic B state of Cl_2 are so large that only a few vibrational periods of the wave packet can be observed in experiments. The anharmonicity of I_2 molecules is much lower. The electronic B state of I_2 in RGS shows rich vibrational wave packet structure. An enormous amount of pump-probe spectroscopy has been done by Apkarian and coworkers [21–24] and the Schwentner group [20, 25–28]. The Coherent Raman Antistokes Scattering (CARS) however indicates a limited electronic coherence $T^{\mathrm{el}}_{\mathrm{deph}}$ time of less than 100 fs in the B $\longleftarrow$ X transition [29–34]. Some of the control methods conducted here will need an electronic coherence time of several hundred femtoseconds and therefore, the B state of the I_2:RGS system cannot be used. However, coherent phonon dynamics and an example of coherent spin-flip will be presented for the I_2:Kr system. The electronic ground state X of I_2 in RGS is not of interest for this study, since the CARS spectra indicate a vibrational dephasing time of several hundred picoseconds, much too long in comparison to complex systems.

Combining the preconditions, we conclude that Br_2 in solid Ar should fulfill all requirements. Excitation spectra of the B $\longleftarrow$ X transition indicate an electronic dephasing of some hundred femtoseconds. The anharmonicity of the B state is in a convenient range that allows for the observation of a few vibrational wave packet periods without major broadening due to dispersion. From the experiments we found that the vibrational dephasing in the electronic B state is in the picosecond domain. Throughout the thesis, the methods and concepts are primarily conducted on the system Br_2 in solid argon.

The ultrafast dynamics of Br_2 has only been studied in two experiments for the free molecule case [35, 36]. Results on ultrafast dynamics of Br_2 in condensed media have not been documented; this thesis presents the first ones. The potential energy surfaces of free Br_2 are documented in literature [37–52]. The electronic potential surfaces can be approximated by Morse potentials very well [53]. The covalent states of Br_2:RGS were studied in absorption and emission spectroscopy [54–66]. The spectra of the charge-transfer states, needed to establish a pump-probe scheme, have been measured by us and are presented in chapters 5 and 6.

To detect the ultrafast vibrational dynamics of the molecule in its environment, the femtosecond pump-probe spectroscopy is applied. By use of a first femtosecond laser pulse (pump), a coherent superposition of vibrational eigenstates (vibrational wave packet) in an excited electronic state (described by a Morse potential) is created. The interference of the vibrational wave functions is interrogated with a second time delayed fs laser pulse (probe).

The wave packet disperses on the Morse oscillator potential of Br_2, since it spans over a

finite range in energy, all of which give rise to different oscillation periods. However, due to the discrete structure of the vibrational levels, the wave packet will revive after some time T_{rev} (determined by the anharmonicity) and regain its narrow shape. The phenomenon is known under the term revival [67–75]. If the vibrational dephasing time $T_{\mathrm{deph}}^{\mathrm{vib}}$ of the molecule in the RGS is larger than the revival time, the decay of coherence among the vibrational eigenstates can be deduced from the pump-probe spectra directly as a decay of revival features [76–78]. If the vibrational dephasing time is shorter than the revival time but larger than the oscillation period T, a new scheme, which is presented in this thesis and a supplementary article [79] has to be applied. The dispersion reduces the modulation contrast on the same timescale as dephasing does. However, dispersion can be suppressed at a distinct time T_{opt} in the evolution by excitation with a negatively chirped pulse (see section 2.2.2). The method has been used before to demonstrate the possibility of vibrational wave packet focusing [80–83]. The scheme will be systematically applied in this thesis to suppress dispersion at a given time T_{opt} and deduce the vibrational dephasing from a background at T_{opt} in the experimental pump-probe spectra (see sections 2.3.3 and 8.2.1).

Apart from full revivals of the vibrational wave packets in Morse oscillators, fractional revivals arise that cause multiples of the fundamental oscillation frequency in the pump-probe spectrum. Using the fractional revivals, information about coherence of a distinct group of vibrational levels can be deduced. Here, the measured vibrational dephasing time $T_{\mathrm{deph}}^{\mathrm{vib}}$ is too short to observe fractional revivals directly. Therefore, a novel scheme to control the fractional revivals of a vibrational wave packet based on chirped excitation pulses is worked out (see section 2.3.4). The revival features are shifted towards the time-zero by a positively chirped excitation pulse. A 1/6 revival, exhibiting the threefold vibrational period, is observed on the B state of Br_2 in solid Ar. From this experiment, a coherence time of four vibrational levels is estimated in section 8.2.2.

The positively chirped excitation pulses used to advance the revival structures in time are actually longer than one oscillation period of the molecule in its excited electronic state. The vibrational wave packet portions created by the first part of the pulse will interfere with the later created parts of the wave packet. Therefore, the electronic coherence between ground and excited state is involved in the coherent preparation of the wave packet (see section 8.2.3). From the pulse duration an electronic coherence time for the B $\longleftarrow$ X transition of Br_2 in solid Ar is estimated.

The coherent vibrational dynamics is used to deduce a detailed picture of the molecule-host interaction. We are able to construct an effective intramolecular B state potential for Br_2 in solid Ar in section 8.1.2. Furthermore, the vibrational energy relaxation of wave packets on the electronic B state is determined (section 8.1.3) and a representative trajectory of a vibrational wave packet is shown (section 8.1.4). For the case of I_2:Kr, the vibrational coherence even survives vibrational energy losses of 1 eV connected to a spin-flip transition to another electronic state (section 8.1.4).

It will turn out that the interaction of the vibrating molecule with the matrix is not necessarily statistical. In contrast, collisions of the molecule with the matrix can lead to the creation of coherent wave packets built from vibrational levels not populated before the collision.

Coherent motions are found even for host atoms, showing up in the pump-probe spectra of the molecular guest. The conflictive issues of the specific mode, together with its excitation and probe mechanism were discussed in [24,29,30,32,84–86]. We attribute the coherent host motion to a Zone Boundary Phonon (ZBP) of the rare gas crystal. To support assignment, spectra of I_2:Kr (also measured by the author) are presented alongside the spectra of Br_2:Ar, both showing the coherent ZBP signature. The excitation of the coherent host phonon is achieved via the

expansion of the molecular electronic cloud during the A ⟵ X or B ⟵ X transition. This scheme is very similar to the model of Displacive Excitation of Coherent Phonons (DECP) [87–95] and will be presented in section 8.3.1. Many different phonon modes are excited, but only the ZBP having a vanishing group velocity stay at the excited molecule. They change the local density in the vicinity of the chromophore and thereby change the solvation energy of the molecular charge-transfer states [86, 96, 97], which in turn modulates the probe transition efficiency (see section 8.3.2).

Several theory groups treat the halogen in RGS systems extensively and their efforts have, to a large extent, motivated our experiments. Classical and quantum mechanical simulations mostly based on the DIM (Diatomics In Molecules) [98–103] approach give a detailed picture of the dynamical processes of molecular guests in a RGS host. Besides calculations on small molecules F_2, HCl, and Cl_2 in rare gases [104–108], simulations of the heavier I_2 molecules in rare gas environments exist [109–116]. Up to now, no simulations of the Br_2 in RGS have been published. Due to the results presented in this thesis, a collaborative effort within the Sfb 450[2] with the groups of Prof. Manz and Prof. Gerber aims to perform such calculations.

This thesis is organized as follows:

Chapter 2 introduces the basic ideas of coherence, dephasing, dispersion and fractional revivals. Furthermore, the ultrafast pump-probe spectroscopy and the methods used to determine vibrational and electronic dephasing times are explained.

The potential energy surfaces of the free Br_2 molecule and the general effects of the RGS on the spectroscopic molecular properties are presented in chapter 3. The experimental setup is described in chapter 4, together with a summary of ultrashort (chirped) laser pulses. The chapters 5, 6 on absorption and emission spectroscopy provide the information needed to conduct fs pump-probe spectroscopy on the system Br_2:Ar.

Chapter 7 presents the first results on Br_2:Ar dynamics, where one- and two-photon probe processes are used to detect vibrational wave packet dynamics. The rotation of the molecule is proved to be frozen. Furthermore, the coherent host motion in Br_2:Ar and I_2:Kr is illustrated.

The vibrational wave packet dynamics is used to determine an effective molecule-matrix potential for the electronic B state of Br_2 in solid Ar in chapter 8.1. Furthermore, the vibrational energy relaxation and an experimental trajectory are calculated in this section. The results on vibrational and electronic dephasing in Br_2:Ar are discussed in chapter 8.2. This chapter ends with the discussion of the coherent zone boundary phonon in I_2:Kr and Br_2:Ar (chapter 8.3).

[2]The collaborative research center SFB 450 is also financing and supporting this experimental work.

Chapter 2

Concepts and methods

Part 2.1 of this chapter will introduce the concepts of coherence, which is a central issue in this thesis. This will be followed by a presentation of dispersion, wave packet focusing and fractional revivals in section 2.2. The pump-probe method and the wave packet control schemes are presented in the final section 2.3 of this chapter.

2.1 Coherence

This section will provide the definition of coherence needed throughout the thesis. It is necessary to have the ideas of coherence in mind to follow the sections to come.

It is reasonable to start from the classical idea of coherence, defined for an ensemble of trajectories in phase space. For convenience, the dephasing and dissipation processes will be explained using a harmonic oscillator potential. The step from classical coherence to quantum coherence is made with the help of the density operator. Since the harmonic approximation is not sufficiently accurate for diatomic molecular electronic potentials, the Morse potential and the propagation of classical trajectories and quantum mechanical wave packets on it will be discussed afterwards. This will lead to the definition of dispersion and fractional revivals of a vibrational wave packet.

2.1.1 Classical coherence

The electronic state of a diatomic molecule is presented in the harmonic approximation. The molecules are elongated from the equilibrium distance (for example in an optical transition) and an oscillatory motion of the molecular ensemble sets in. The classical molecular ensemble shall have a finite width in the spatial distribution, inducing also a finite width in the momentum distribution. The ensemble is represented in phase space. One dimension describes the elongation q of the oscillators, the other dimension the momentum p. The distribution of oscillators is represented as a grey shaded area in phase space as shown in Fig. 2.1.

The molecules are considered as oscillating freely in Fig. 2.1a. The q and p axis of phase space shall be scaled such that q^2 represents the potential energy and p^2 the kinetic energy. For that case the total energy is given by $r^2 = q^2 + p^2$, where r is the distance to phase space origin. Since the energy of each oscillator is conserved, the value of r is not changed in the propagation. Apart from this, the angle α which the ensemble spans from the phase space origin is also not changed in the course of time. The propagation is said to be completely coherent in the case described in Fig. 2.1a.

Next, statistical elastic collisions with an environment are introduced. The molecular oscillators will not lose any vibrational energy in the collision, but the phase of an individual oscillator is changed by a small random value. The molecular oscillator will jump to another position in phase space, nevertheless keeping the same energy (*i.e.* r^2). The change of the molecular ensemble in this *dephasing* process is shown in Fig. 2.1b. The angle α gets broader in the

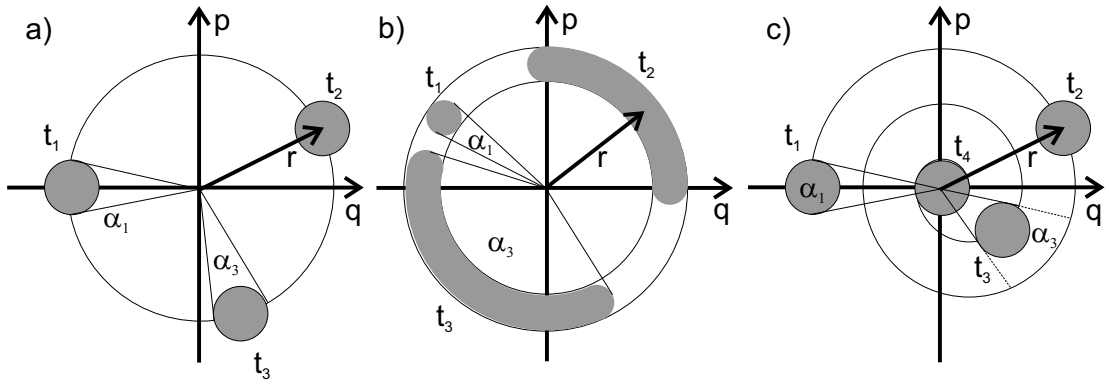

Figure 2.1: a) An ensemble of free classical harmonic oscillators in phase space position (q, p)(position,momentum) is shown as the grey area. No dephasing or dissipation occurs and the angle α under which the ensemble is seen from the origin of phase space does not change in the course of time (t_1< t_2<t_3). The radius r being proportional to the average energy is also constant in time. b) Case of pure dephasing. The molecules suffer statistical elastic collisions with an environment. The phase of a single molecular oscillator is changed by a small random value in a collision. The angle α for the ensemble average grows with propagation time (α_1 < α_3). c) Dissipative case. The molecules suffer inelastic collisions with a bath. The absolute width of the ensemble shall not be changed (no pure dephasing). The mean energy decreases as a function of time and the ensemble spirals to the potential minimum in the origin of the phase space plot. Furthermore, α increases with time, indicating the connection of dissipation and dephasing (form Ref. [73]).

course of time, with $\alpha_3 > \alpha_1$ for ($t_3 > t_1$). With increasing time, the molecular oscillator ensemble will fill the complete iso energetic ring depicted in Fig. 2.1b with a corresponding angle $\alpha = 2\pi$. Such an ensemble would be called completely incoherent or completely "*dephased*". Each molecule would still fulfill a harmonic oscillation, but its phase cannot be predicted, since the elastic collisions occur statistically. The same effect would occur, if the oscillation frequency would be slightly different for the groups of molecules. For example, some molecules can be heavier than others, as is the case for different molecular isotopes. Such a broadening of the angle α due to a splitting of the ensemble in groups with different oscillatory properties will be called in general *inhomogeneous*, while broadening effects being the same for every member will be generally called *homogenous*.

Apart from elastic collisions, inelastic collisions also occur in the investigation. The effect is called *dissipation*, or in the special case described in this thesis vibrational energy relaxation, and is illustrated in Fig. 2.1c. The molecular ensemble loses energy and spirals towards the center of phase space. The molecular ensemble propagates to smaller distances in r but keeps the width in q and p, since the phase of an individual oscillator is not changed. Connected with the loss of energy is the broadening of the angle α. Therefore, dephasing is directly connected to dissipation and cannot be avoided. When the vibrational ensemble has relaxed to the center of phase space, α is equal to 2π. To distinguish the dephasing induced by dissipation (Fig. 2.1c) from the dephasing described in Fig. 2.1b, the latter is often called *pure dephasing*.

The classical coherence introduced above can indeed be used to describe many experiments. Apkarian and coworkers, for example, have used classical trajectories for a calculation of pump-probe experiments [22–24]. However, the interference phenomena cannot be simulated in the classical approach. The quantum coherence is therefore introduced in the next section. The picture developed for a completely classical ensemble of molecules deserves to introduce the

term of quantum coherence here.

2.1.2 Quantum coherence

The nth eigenfunction $|\phi_n\rangle$ in a potential shall belong to energy eigenvalue E_n. A wave packet $|\Psi(t)\rangle$ can be written as a superposition of energy eigenfunctions :

$$|\Psi(t)\rangle = \sum_n c_n e^{-i\frac{E_n}{\hbar}t}|\phi_n\rangle, \tag{2.1}$$

where c_n are the excitation coefficients. The $|\phi_n\rangle$ can be vibrational, rotational or electronic eigenfunctions of the molecule.

In order to define the quantum coherence properly, one has to consider the density operator ρ:

$$\rho = \sum_i p_i |\Psi_i\rangle\langle\Psi_i|. \tag{2.2}$$

$|\Psi_i\rangle$ is a wave function or wave packet. The p_i are the statistical probabilities of finding the system in the state $|\Psi_i\rangle$. They have to fulfill the condition:

$$\sum_i p_i = 1.$$

The state is called *pure*, if there is one i for which p_i = 1 and all the other p_j = 0 ($i \neq j$). In any other case, the state is said to be *mixed*. Let $\rho(x', x)$ be the density operator in the position representation of $|\Psi(t)\rangle$, which is a wave packet according to Eq. (2.1). Then:

$$\begin{aligned}
\rho(x', x) &= \langle x'|\Psi(t)\rangle\langle(t)\Psi|x\rangle \\
&= \sum_{m,n}\langle x'|\phi_m\rangle\langle\phi_m|\Psi(t)\rangle\langle(t)\Psi|\phi_n\rangle\langle\phi_n|x\rangle \\
&= \sum_{m,n}\phi_m(x')(c_m\mathrm{e}^{-\frac{\mathrm{i}}{\hbar}\mathrm{E_m t}})(\mathrm{c_n^*e}^{+\frac{\mathrm{i}}{\hbar}\mathrm{E_n t}})\phi_\mathrm{n}^*(\mathrm{x}) \\
&= \sum_{m,n}\phi_m(x')\rho_{mn}\phi_n^*(x),
\end{aligned} \tag{2.3}$$

with $\rho_{mn} = c_m c_n^* e^{-\frac{i}{\hbar}(E_m - E_n)t}$ being the density operator (matrix) in the energy representation. A simple example to illustrate ρ_{mn} shall be given in a two-state system:

$$\rho_{mn} = \begin{pmatrix} |c_1|^2 & c_1 c_2^* e^{-\frac{i}{\hbar}(E_1 - E_2)t} \\ c_1^* c_2 e^{-\frac{i}{\hbar}(E_2 - E_1)t} & |c_2|^2 \end{pmatrix} \tag{2.4}$$

The diagonal elements of the density matrix are called populations. The off-diagonal elements are called quantum *coherences*. In contrast to the diagonal elements, they are complex and oscillate in time with a frequency corresponding to the energy difference.

These coherences are crucial for the development of interference patterns between the different eigenfunctions, as shall be explained for a system consisting of two vibrational eigenfunctions $\phi_0(R)$ and $\phi_1(R)$ with energies $E_0 = \frac{1}{2}\omega_e$ and $E_1 = \frac{3}{2}\omega_e$. The wave packet is written as: $\Psi(R,t) = c_0\mathrm{e}^{-\mathrm{i}\omega_\mathrm{e}(0+\frac{1}{2})\mathrm{t}}\phi_0(\mathrm{R}) + \mathrm{c_1 e}^{-\mathrm{i}\omega_\mathrm{e}(1+\frac{1}{2})\mathrm{t}}\phi_1(\mathrm{R})$. One obtains the probability density: $|\Psi(R,t)|^2 = |c_0|^2|\phi_0(R)|^2 + |c_1|^2|\phi_1(R)|^2 + 2Re(c_0^* c_1 \phi_0^*(R)\phi_1(R)e^{-i/(E_1 - E_0)t/\hbar})$. The interference term in the last equation is is based on the real part of the coherence of the density